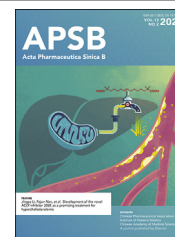




Chinese Pharmaceutical Association  
Institute of Materia Medica, Chinese Academy of Medical Sciences

Acta Pharmaceutica Sinica B

[www.elsevier.com/locate/apsb](http://www.elsevier.com/locate/apsb)  
[www.sciencedirect.com](http://www.sciencedirect.com)



ORIGINAL ARTICLE

# (+)/(–)-Yanhusamides A–C, three pairs of unprecedented benzylisoquinoline-pyrrole hetero-dimeric alkaloid enantiomers from *Corydalis yanhusuo*

Lingyan Wang<sup>a,b,†</sup>, Guiyang Xia<sup>a,†</sup>, Huan Xia<sup>a</sup>, Xiaohong Wei<sup>a</sup>, Yanan Wang<sup>b</sup>, Sheng Lin<sup>a,\*</sup>

<sup>a</sup>Key Laboratory of Chinese Internal Medicine of Ministry of Education and Beijing, Dongzhimen Hospital, Beijing University of Chinese Medicine, Beijing 100700, China

<sup>b</sup>State Key Laboratory of Bioactive Substance and Function of Natural Medicines, Institute of Materia Medica, Chinese Academy of Medical Sciences and Peking Union Medical College, Beijing 100050, China

Received 31 August 2022; received in revised form 30 September 2022; accepted 19 October 2022

## KEY WORDS

(+)/(–)-Yanhusamides A–C;  
Hetero-dimeric alkaloids;  
*Corydalis yanhusuo*;  
Anti-inflammatory;  
Analgesic activity

**Abstract** A chemical investigation on the aqueous extract of *Corydalis yanhusuo* tubers led to the isolation and structural elucidation of three pairs of trace enantiomeric hetero-dimeric alkaloids, (+)/(–)-yanhusamides A–C (**1–3**), featuring an unprecedented 3,8-diazatricyclo[5.2.2.0<sup>2,6</sup>]undecane-8,10-diene bridged system. Their structures were exhaustively characterized by X-ray diffraction, comprehensive spectroscopic data analysis, and computational methods. Guided by the hypothetical biosynthetic pathway for **1–3**, a gram-scale biomimetic synthesis of (±)-**1** was achieved in 3 steps using photoenolization/Diels–Alder (PEDA) [4+2] cycloaddition. Compounds **1–3** exhibited potent inhibition of NO production induced by LPS in RAW264.7 macrophages. The *in vivo* assay showed that oral administration of 30 mg/kg of (±)-**1** attenuated the severity of rat adjuvant-induced arthritis (AIA). Additionally, (±)-**1** induced a dose-dependent antinociceptive effect in the acetic acid-induced mice writhing assay.

© 2023 Chinese Pharmaceutical Association and Institute of Materia Medica, Chinese Academy of Medical Sciences. Production and hosting by Elsevier B.V. This is an open access article under the CC BY-NC-ND license (<http://creativecommons.org/licenses/by-nc-nd/4.0/>).

\*Corresponding author.

E-mail address: [lszm@bucm.edu.cn](mailto:lszm@bucm.edu.cn) (Sheng Lin).

<sup>†</sup>These authors made equal contributions to this work.

Peer review under responsibility of Chinese Pharmaceutical Association and Institute of Materia Medica, Chinese Academy of Medical Sciences.

<https://doi.org/10.1016/j.apsb.2022.10.025>

2211-3835 © 2023 Chinese Pharmaceutical Association and Institute of Materia Medica, Chinese Academy of Medical Sciences. Production and hosting by Elsevier B.V. This is an open access article under the CC BY-NC-ND license (<http://creativecommons.org/licenses/by-nc-nd/4.0/>).



## 1. Introduction

Dimeric natural products (DNPs), including homo- and hetero-dimers derived from the polymerization of two identical and different monomers, respectively, have attracted dramatically increasing attention in recent years because of their high structural complexity and significant bioactivities<sup>1–4</sup>. Strikingly, the DNPs usually display more potent bioactivities than their corresponding parent monomers. Indeed, some DNPs have been developed as well-known therapeutic agents, such as the antimicrobial agent hypericin<sup>5,6</sup>, anticancer agents vinblastine and vincristine<sup>7</sup>, anti-mitotic podophyllotoxin<sup>8</sup>, and immunosuppressant gossypol<sup>9</sup>.

The plants of Berberidaceae, Menispermaceae, Papaveraceae, Euphorbiaceae, and Ranunculaceae family are rich sources of dimeric alkaloids, especially the bisbenzyloquinoline alkaloids (BBIAs) assembled from two monomeric benzyloquinoline alkaloids (BIAs) *via* one or two C–O–C or C–C bond connections<sup>10–14</sup>. Remarkably, some BBIAs have been reported to reverse multidrug resistance and inhibit 2019 novel coronavirus (2019-nCoV) and Ebola virus<sup>15,16</sup>. Inspired by the explorations of dimeric alkaloids with novel structures as potential drug leads, our recent chemical exploration of an aqueous extract of *Corydalis yanhusuo* tubers, which is best known as a traditional Chinese medicine (TCM) “*yuan hu*” utilized in treating spasms, menstrual and abdominal pain, dysmenorrhea, rheumatism, gastric ulcers, myocardial ischemia, and cardiac arrhythmias<sup>17,18</sup>, revealed two unique C–C coupled type of dimeric BIAs with inhibitory activity against PD-1/PD-L1 interaction and anti-inflammatory activities<sup>19,20</sup>. This motivated us to continue chemical investigations of this fraction, which resulted in the discovery of three pairs of trace novel hetero-dimeric alkaloid enantiomers, (+)/(–)-yanhusamides A (**1**), B (**2**), and C (**3**). Structurally, the motif of (+)/(–)-yanhusamides A–C (**1–3**), which is the first example of benzyloquinoline-pyrrole dimeric alkaloids generated *via* Diels–Alder reaction by coupling coptisine with *N*-acetyl dihydropyrrole or 1,3-dihydro-2*H*-pyrrol-2-one, possess an unprecedented 3,8-diazatricyclo[5.2.2.0<sup>2,6</sup>]undecane-8,10-diene core (Fig. 1). Subsequent biomimetic syntheses of **1** readily construct this novel motif by a concise scheme using photoenolization/Diels–Alder (PEDA) [4+2] cycloaddition reaction.

Pain is a significant symptom associated with many musculoskeletal conditions leading to functional impairment and poor

quality of life<sup>21</sup>. Rheumatoid arthritis (RA), characterized by massive pain and destruction of synovial joints, is an inflammatory autoimmune disease that generally necessitates lifelong therapy<sup>22</sup>. It has been reported that the level of NO in the serum and synovial fluid of patients with RA has been shown to be significantly increased. Inducible NOS inhibitors have been found to significantly reduce the NO production associated with rat AIA<sup>23</sup>. Disease-modifying antirheumatic drugs (DMARDs) are common drugs to relieve the symptoms of RA. However, various side effects of these drugs limited their clinical application<sup>24</sup>. Apart from western medicines, TCMs are also well accepted for pain management, and the title TCM “*yuan hu*” is famous for its antalgic and anti-inflammatory efficacy. Thus, the evaluation of the *in vitro* anti-inflammatory properties of **1–3**, and *in vivo* anti-arthritis and analgesic activities of **1** were carried out.

Herein, we describe details of their isolation, structural elucidations, plausible biogenesis, biomimetic synthesis, and the anti-inflammatory and analgesic effects *in vitro* and *in vivo*.

## 2. Results and discussion

### 2.1. Structural elucidation of compounds **1–3**

Yanhusamide A (**1**) was obtained as a yellow, amorphous powder. Its molecular formula, C<sub>25</sub>H<sub>23</sub>N<sub>2</sub>O<sub>5</sub>, was established by its positive HRESIMS at *m/z* 431.1597 [M]<sup>+</sup> (Calcd. for C<sub>25</sub>H<sub>23</sub>N<sub>2</sub>O<sub>5</sub>, 431.1602) along with the <sup>1</sup>H and <sup>13</sup>C NMR data. The presence of carbonyl (1681 cm<sup>–1</sup>), imine (1628 cm<sup>–1</sup>), and aromatic ring (1586, 1509, and 1468 cm<sup>–1</sup>) functionalities in the structure of **1** was revealed from the diagnosable absorption bands in the IR spectrum. The <sup>1</sup>H NMR spectrum of **1** disclosed characteristic signals of two moieties: a 1,6,7-trisubstituted tetrahydroisoquinoline moiety was evidenced by the resonances at δ<sub>H</sub> 3.13 (1H, ddd, *J* = 16.8, 10.8, 6.6 Hz), 3.25 (1H, ddd, *J* = 16.8, 8.4, 6.6 Hz), 4.16 (1H, ddd, *J* = 15.0, 8.4, 6.6 Hz), 4.33 (1H, ddd, *J* = 15.0, 10.8, 6.6 Hz), 7.03 (1H, s), and 7.80 (1H, s); a 1,2,3,4-tetrasubstituted phenyl substructure was indicated by the *ortho*-coupled proton resonances at δ<sub>H</sub> 6.97 (1H, d, *J* = 7.8 Hz) and 6.93 (1H, d, *J* = 7.8 Hz). These assignments were in accordance with the <sup>13</sup>C NMR data and supported by the 2D NMR experiments (Table 1 and Fig. 2). Further, the DEPT and HSQC data of **1** confirmed the presence of two methylenedioxy moieties [δ<sub>H</sub> 6.23, 6.21 (each 1H, s) and 6.14, 6.11 (each 1H, s); δ<sub>C</sub> 105.0 and 104.0], and their positions were located in the phenyl rings at C-2/C-3 and C-9/C-10, respectively, which was supported by the key HMBC correlations that was depicted in Fig. 2. Based on these data and 16 indexes of hydrogen deficiency inherent in the molecular formula of **1**, it was revealed that **1** was a tetrahydrocoptisine-alkaloid derivative containing eight ring systems.

Comparisons of the 1D and 2D NMR spectra of **1** with those of the co-isolated benzyloquinoline-derived alkaloids presented several intriguing structural differences in the low- and middle-field region of the <sup>1</sup>H and <sup>13</sup>C NMR spectra<sup>17,25</sup>. These differences consisted of signals for four methines [CH-8 (δ<sub>H</sub> 5.78; δ<sub>C</sub> 64.5), CH-13 (δ<sub>H</sub> 5.80; δ<sub>C</sub> 46.0); CH-2' (δ<sub>H</sub> 4.63, δ<sub>C</sub> 60.2); CH-3' (δ<sub>H</sub> 3.38, δ<sub>C</sub> 44.1)], two methylenes [CH<sub>2</sub>-4' (δ<sub>H</sub> 2.23 and 1.65, δ<sub>C</sub> 27.1) and CH<sub>2</sub>-5' (δ<sub>H</sub> 3.43 and 1.94, δ<sub>C</sub> 48.9)], and an acetyl group (δ<sub>H</sub> 1.93, δ<sub>C</sub> 172.0 and 22.5). Among these signals, an *N*-

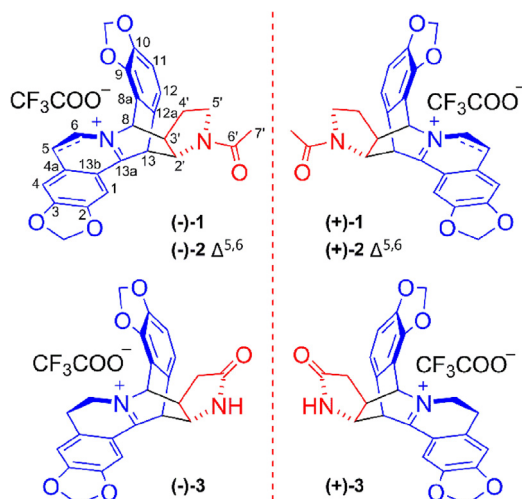


**Figure 1** Structures of (+)/(–)-yanhusamides A–C [(+)/(–)-**1–3**].

acetyldihydropyrrole was drawn based on  $^1\text{H}$ - $^1\text{H}$  COSY homonuclear vicinal coupling correlation peaks of H-2'/H-3'/H<sub>2</sub>-4'/H<sub>2</sub>-5' and HMBC correlation signals from H-2' to C-4'/C-5'/C-6', from H-3' to C-5', and from H<sub>2</sub>-5' to C-2'/C-6'. In addition, the remaining two methines at  $\delta_{\text{H}}$  5.78 (H-8) and 5.80 (H-13) involved in two COSY spin systems corresponding to H-8/H-3' and H-13/H-2', and showed  $^1\text{H}$ - $^{13}\text{C}$  HMBC correlation peaks of H-8 to C-12a/C-13/C-13a/C-2'/C-4', and of H-13 to C-8a/C-3'. These observations, coupled with the important HMBC correlations from H-3' to C-8a/C-13, and from H-2' to C-8/C-12a/C-13a, served to construct a 3,8-diazatricyclo[5.2.2.0<sup>2,6</sup>]undecane-8,10-diene ring system in **1**. Finally, the HMBC cross-peaks of H-8/C-6, H-8/C-9, H<sub>2</sub>-6/C-8, H-13/C-13b, and H-12/C-13, justified the fusion of the tetrahydrocoptisine moiety and the acetyldihydropyrrole unit *via* C-3'-C-8 and C-2'-C-13 to form the 3,8-diazatricyclo[5.2.2.0<sup>2,6</sup>]undecane-8,10-diene ring system, thereby completing the unique gross structure of **1** shown in Fig. 1.

The rigid conformation of **1** readily allowed the three-dimensional arrangement of the rings to be present. The NOESY correlations of H-1/H-2' and H-12/H-5'b indicated that the *N*-acetyldihydropyrrole ring is in a *cis* relationship with 1,2,3,4-tetrasubstituted phenyl ring and possesses a *trans* relationship to the tetrahydroisoquinoline ring system illustrated in Fig. 3A. This deduction was affirmed by the  $^{13}\text{C}$  NMR chemical shift calculations for the two constructed diastereomers,

8*S*\*,13*S*\*,2'*S*\*,3'*R*\*-**1** and 8*R*\*,13*R*\*,2'*S*\*,3'*R*\*-**1**, of which the 8*S*\*,13*S*\*,2'*S*\*,3'*R*\*-**1** met well with the experimental data and got a high DP4+ probability of 99.88% (Fig. 3B). After several attempts, a qualified crystal, which was suitable for the testament of single-crystal X-ray diffraction, was cultivated from a multivariate solvent system (MeOH/H<sub>2</sub>O/HNO<sub>3</sub>, 9:1:0.1), and the ultimate proof of the structural construction of **1**, including the relative configuration, was confirmed by the X-ray data (CCDC 2201234) of **1**, but existing as a racemic mixture (Fig. 3C). This readily explained that the optical activity of yanhusamide A (**1**) was measured to be 0, and the ECD spectrum is a line. Fortunately, **1** was successfully separated by chiral-phase HPLC that was equipped with an IB-N3 chiral column to afford the anticipated enantiomers (-)-**1** and (+)-**1**, which showed mirror-like ECD spectra and fully opposite optical rotations (Supporting Information Figs. S20 and S21). Therefore, the comparison of the experimental and computational electronic circular dichroism (ECD) spectra was employed to determine the absolute configurations of (-)-**1** and (+)-**1** (Fig. 4). The ECD spectra calculated for 8*S*,13*S*,2'*S*,3'*R*-**1** and 8*R*,13*R*,2'*R*,3'*S*-**1** matched well with those measured for (-)-**1** and (+)-**1**, respectively, which also could be successfully interpreted by the ECD exciton chirality rule induced by the two chromophores of tetrahydroisoquinoline moiety and benzene ring (Fig. 4). Thus, the stereochemistry of (-)-**1** and (+)-**1** were proved to be 8*S*,13*S*,2'*S*,3'*R* and 8*R*,13*R*,2'*R*,3'*S*, respectively. Yanhusamide A (**1**) was expected to

**Table 1**  $^1\text{H}$  and  $^{13}\text{C}$  NMR data for ( $\pm$ )-**1**-**3** in MeOH-*d*<sub>4</sub>.

No.	( $\pm$ )- <b>1</b>		( $\pm$ )- <b>2</b>		( $\pm$ )- <b>3</b>	
	$\delta_{\text{H}}$ ( <i>J</i> in Hz) <sup>a</sup>	$\delta_{\text{C}}$ <sup>b</sup>	$\delta_{\text{H}}$ ( <i>J</i> in Hz) <sup>a</sup>	$\delta_{\text{C}}$ <sup>b</sup>	$\delta_{\text{H}}$ ( <i>J</i> in Hz) <sup>a</sup>	$\delta_{\text{C}}$ <sup>b</sup>
1	7.80 s	109.8	8.19 s	102.8	7.81 s	109.7
2		150.0		154.2		150.0
3		158.0		158.4		158.1
4	7.03 s	110.5	7.57 s	105.1	7.04 s	110.5
4a		138.1		140.5		138.3
5	3.25 ddd (16.8, 8.4, 6.6) 3.13 ddd (16.8, 10.8, 6.6)	27.3	8.08 d (6.6)	123.8	3.26 ddd (16.8, 8.4, 6.6) 3.15 ddd (16.8, 10.8, 6.6)	27.3
6	4.33 ddd (15.0, 10.8, 6.6) 4.16 ddd (15.0, 8.4, 6.6)	49.2	8.66 d (6.6)	132.7	4.34 ddd (15.0, 10.8, 6.6) 4.17 ddd (15.0, 8.4, 6.6)	49.6
8	5.78 d (3.6)	64.5	6.53 (3.6)	65.2	5.77 d (3.6)	64.1
8a		115.5		115.3		114.2
9		145.0		145.3		145.6
10		150.0		149.8		149.8
11	6.93 d (7.8)	110.2	6.93 d (7.8)	110.4	6.92 d (7.8)	110.0
12	6.97 d (7.8)	120.7	7.03 d (7.8)	120.6	7.04 d (7.8)	121.8
12a		127.5		129.3		126.9
13	5.80 d (3.6)	46.0	6.17 d (3.6)	43.5	5.40 d (3.6)	48.1
13a		176.2		154.6		175.9
13b		118.6		124.7		118.5
2'	4.63 dd (8.4, 3.6)	60.2	4.63 dd (8.4, 3.6)	60.4	4.27 dd (8.4, 3.6)	55.9
3'	3.38 m	44.1	3.34 m	44.4	3.43 m	38.3
4'a	2.23 ddd (20.4, 13.8, 10.2)	27.1	2.31 ddd (20.4, 13.8, 10.2)	27.2	2.60 dd (18.6, 10.8)	32.9
4'b	1.65 ddt (13.8, 7.8, 1.8)		1.81 ddt (13.8, 7.8, 1.8)		1.80 dd (18.6, 3.6)	
5'a	3.43 td (10.2, 2.4)	48.9	3.50 td (10.2, 2.4)	48.9		178.0
5'b	1.94 td (10.2, 7.8)		2.10 td (10.2, 7.8)			
6'		172.0		172.1		
7'	1.93 s	22.5	1.98 s	22.6		
2,3-OCH <sub>2</sub> O-	6.23 s	105.0	6.41 s	105.8	6.23 d (1.2)	105.1
	6.21 s		6.39 s		6.21 d (1.2)	
9,10-OCH <sub>2</sub> O-	6.14 s	104.0	6.17 d (1.2)	104.1	6.13 d (1.2)	104.1
	6.11 s		6.09 d (1.2)		6.10 d (1.2)	

<sup>a</sup> $^1\text{H}$  NMR data ( $\delta$ ) were measured in 600 MHz NMR instrument. Proton coupling constants (*J*) in Hz are given in parentheses.

<sup>b</sup>Data were recorded at 150 MHz. The assignments were based on  $^1\text{H}$ - $^1\text{H}$  COSY, HSQC, HMBC, and NOESY experiments.

be obtained as a trifluoroacetate due to the use of trifluoroacetic acid in the HPLC isolation procedure. The  $^{19}\text{F}$  NMR experiment of **1** verified this conclusion based on the presence of a strong  $^{19}\text{F}$  resonance at  $\delta_{\text{F}} -76.8$  (Supporting Information Fig. S16). Based on these data, (–)-**1** and (+)-**1** were trivially named as (–)-yanhusamide A trifluoroacetate and (+)-yanhusamide A trifluoroacetate, respectively.

Yanhusamide B (**2**) was purified as a yellow amorphous powder. The positive HRESIMS spectrum gave the  $\text{C}_{25}\text{H}_{21}\text{N}_2\text{O}_5$  (Calcd. for  $\text{C}_{25}\text{H}_{21}\text{N}_2\text{O}_5$ , 429.1445) molecular formula, which differed from that of **1** by reducing two hydrogen atoms, from the molecular ion at  $m/z$  429.1443  $[\text{M}]^+$ . It was quickly evident that **2** was simply the olefinic analogue of **1** because the NMR signals for two adjacent methylenes in **1** were replaced by a disubstituted double bond [ $\delta_{\text{H}}$  8.66 (1H, d,  $J = 6.6$  Hz) and 8.08 (1H, d,  $J = 6.6$  Hz;  $\delta_{\text{C}}$  132.7 and 123.8]. Inspection of the 2D NMR ( $^1\text{H}$ – $^1\text{H}$  COSY, HMBC, and NOESY) spectra of **2** confirmed the location of the double bond at C-5/C-6 (Figs. 2 and 3A). Therefore, the structure of **2** was established as shown in Fig. 1.

The key NOESY correlation signals were identical with those in **1** (Fig. 3A), suggesting that **2** had the comparable relative configuration as that of **1**, which was further confirmed by the comparison and DP4+ prediction of the experimental and computational  $^{13}\text{C}$  NMR data of **2** (Fig. 3B). Similarly, **2** was also a pair of enantiomers [(+)/(–)-**2**] and was successfully separated using the IB-N3 column (Supporting Information Fig. S7). Similar to (+)/(–)-**1**, the determination of the stereochemistry of (–)-**2** and (+)-**2** were realized by comparison of the experimental and theoretical ECD spectra and ECD exciton chirality method (Fig. 4). The  $^{19}\text{F}$  NMR of **2** (Supporting Information Fig. S29) indicated that **2** was also a trifluoroacetate. Therefore, the structures of (–)-**2** and (+)-**2** were named as (–)-yanhusamide B trifluoroacetate and (+)-yanhusamide B trifluoroacetate, respectively.

Yanhusamide C (**3**) was also obtained as a yellow amorphous powder. It could be speculated that **3** was an analogue of **1** according to the detailed resolution of 1D and 2D NMR data (Table 1 and Fig. 2). The noteworthy differences in their NMR spectra were ascertained in the pyrrole moiety with the absence of the

acetyl signal, together with the severely downfield shifts of C-5' ( $\Delta\delta_{\text{C}} +129.1$ ) and C-4' ( $\Delta\delta_{\text{C}} +5.8$ ), and upfield shifts of C-2' ( $\Delta\delta_{\text{C}} -4.3$ ) and C-3' ( $\Delta\delta_{\text{C}} -5.8$ ), which resulted in the existence of a 1,3-dihydro-2H-pyrrol-2-one ring in **3**, instead of the *N*-acetyldihydropyrrole ring in **1** and **2**. This was approved by the observation of the key HMBC correlation signals from H<sub>2</sub>-4' to C-2'/C-3'/C-5'/C-8, from H-3' to C-5'/C-8a, as well as from H-2' to C-5'/C-12a. Yanhusamide C (**3**) shared the same relative configuration as **1** and **2**, which was evidenced by the key NOESY cross-peak between H-3' and H-5a (Fig. 3A) and was further confirmed by the  $^{13}\text{C}$  NMR computation (Fig. 3B). Unsurprisingly, **3** was another pair of enantiomers and (–)-**3** and (+)-**3** were successfully separated *via* chiral-phase HPLC in a near 1:1 ratio. Subsequently, the determination of absolute stereo-chemical configurations of (–)-**3** and (+)-**3** were carried out on the base of the comparative analysis of the measured and theoretically calculated ECD curves (Fig. 4). Hence, (–)-**3** and (+)-**3** were accorded the trivial names (–)-yanhusamide C trifluoroacetate and (+)-yanhusamide C trifluoroacetate, respectively.

## 2.2. Plausible biosynthetic pathway of compounds 1–3

For the past few years, natural product enantiomers with unique scaffolds have been continuously isolated from terrestrial fungi and higher plants<sup>26–30</sup>. Structurally, (±)-yanhusamides A–C (**1–3**) were novel benzyloquinoline-derived alkaloids, of which the main feature is the 3,8-diazatricyclo[5.2.2.0<sup>2,6</sup>]undecane-8,10-diene scaffold. This unprecedented scaffold present in **1–3** has no counterpart in natural products. Therefore, the plausible biogenetic pathway for **1–3** is proposed in Scheme 1. The co-occurring coptisine (**4**), which has been abundantly obtained from the dried tuber of *C. yanhusuo*, is proposed to be the biosynthetic precursor of **1–3**. (±)-Yanhusamide A (**1**) and (±)-yanhusamide C (**3**) would be biosynthesized *via* a Diels–Alder (DA) [4+2] cycloaddition by coupling **4** with *L*-ornithine derivatives *N*-acetyldihydropyrrole (**ii**) and 1,3-dihydro-2H-pyrrol-2-one (**iv**), respectively, in two different faces to furnish these distinct bridged heterocyclic scaffolds. Subsequently, (±)-yanhusamide B (**2**) was derived from (±)-**1** *via* dehydrogenation.

## 2.3. Biomimetic synthesis of compound 1

With only trace amounts of the above novel alkaloids obtained, further in-depth pharmacodynamic evaluation was greatly hampered. Nevertheless, the biosynthetic hypotheses offer inspiration for synthesis of these compounds. As gram-scale of the key precursor coptisine (**4**) has been obtained from *C. yanhusuo* in this study, the key precursor **iii** would be obtained through *N*-acetylation of pyrrolidine (**i**) (Scheme 2). However, the intermolecular DA [4+2] cycloaddition between **4** and **iii** is a challenge to overcome as there might be 8 possible adducts. To our delight, a three-step biomimetic synthesis of **1**, involving the use of the key light-triggered click DA reaction at room temperature, has been accomplished.

Firstly, the synthesis of **iii** was achieved as shown in Scheme 2 using known procedures<sup>31–33</sup>. The commercially available **i** was oxidized to **ii** using  $\text{Na}_2\text{S}_2\text{O}_8$  and NaOH in the presence of silver nitrate. As reported, **ii** exists in equilibrium with its cyclo-trimer oligomer (**ix**). Considering that **ix** could be used as a synthetic equivalent of **ii**, the mixture of **ii** and **ix** was applied to the following reaction as such without separation and purification.

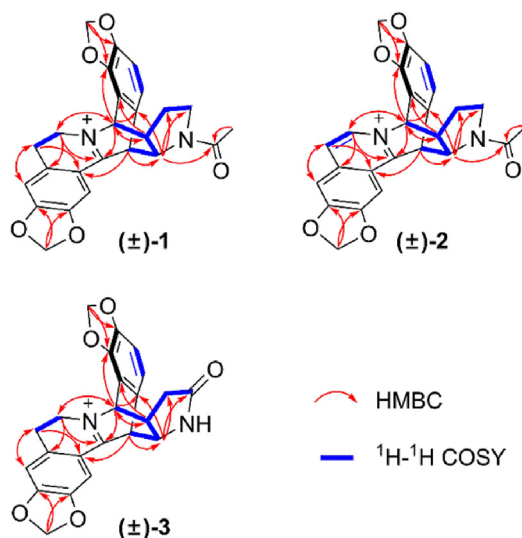


**Figure 2** Main  $^1\text{H}$ – $^1\text{H}$  COSY and HMBC (from  $^1\text{H}$  to  $^{13}\text{C}$ ) correlations of compounds **1–3**.

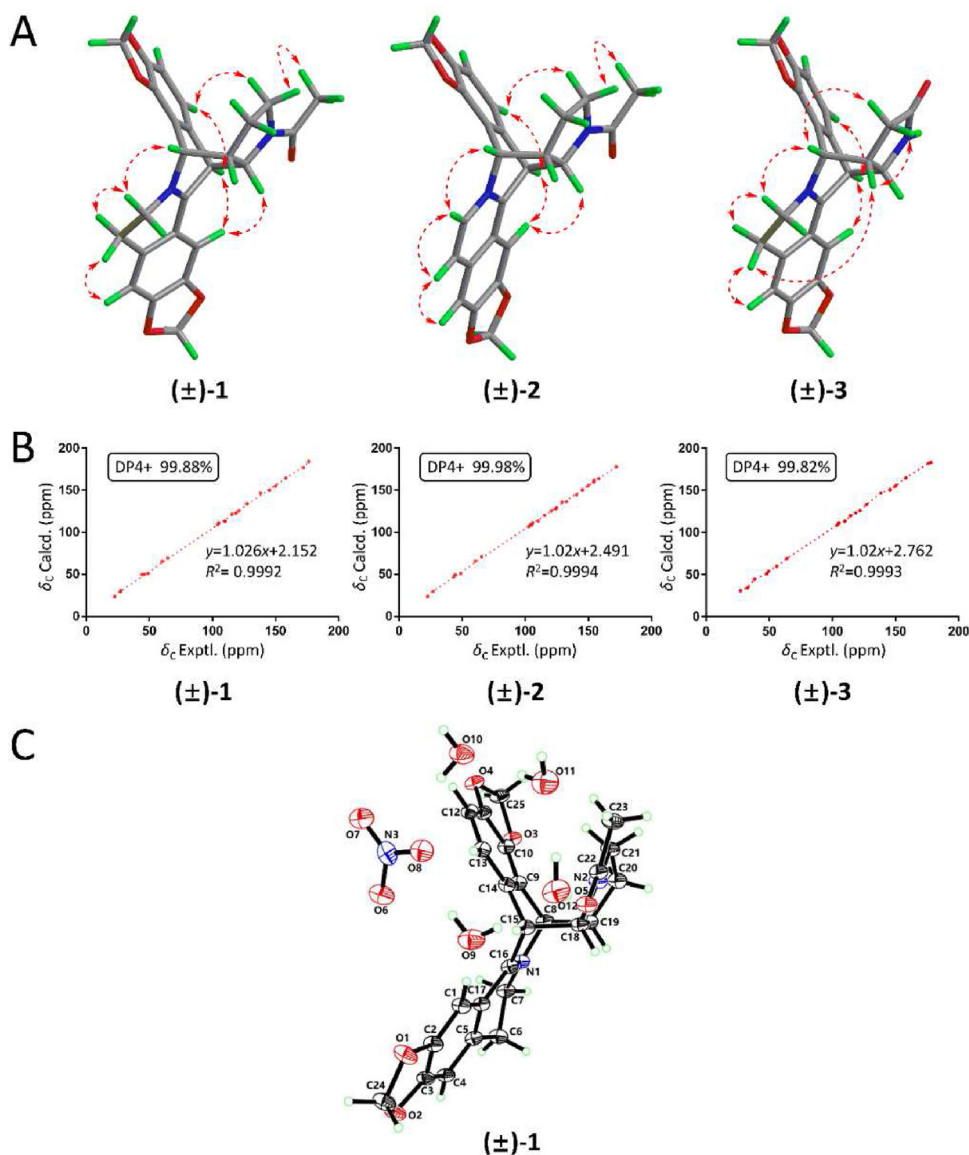


**Figure 3** (A) Energy-minimized conformation with key NOESY correlations for compounds **1**–**3**. (B) Correlation plots of experimental and calculated  $^{13}\text{C}$  NMR data and DP4+ results of compounds **1**–**3**. (C) ORTEP drawing of compound **1**.

Therefore, the mixture of **ii** and **ix** was co-distilled with tetrahydrofuran (THF) and trapped into a flask precooled to  $-78\text{ }^\circ\text{C}$ . The addition of acetic anhydride and Hunig's base (*N,N*-diisopropylethylamine, DIPEA) afforded a 65% yield of **iii**.

DA [4+2] cycloaddition, a well-known textbook reaction, has undergone detailed studies in the formation of a large number of structurally complex natural products<sup>34–36</sup>. Thermal process conditions for the key DA cycloaddition between **4** and **iii** were screened by heating at different temperatures. However, we were disappointed that none of these conditions could allow the formation of the desired DA cycloaddition adducts. We then turned our attention towards the PEDA cycloaddition strategy according to the alternative reaction mechanism<sup>37,38</sup>. As a PEDA reaction could be accessed with a unique wavelength for a specific diene and dienophile system, photoinduced cycloaddition of **4** with **iii** at different wavelengths was conducted at room temperature. The conversion was determined *via* TLC analysis using (±)-**1** as a

reference. Surprisingly, the desired adducts (–)-**1** and (+)-**1** in a near 1:1 ratio, which were confirmed by HPLC–HRMS, NMR, and chiral-phase HPLC analysis, appeared under LED irradiation at 400 and 420 nm, where 400 nm is preferable. Furthermore, increasing yields of (±)-**1** could be observed with the extension of the irradiation time, and a maximum yield of (±)-**1** in 80% from **4** was achieved after irradiation at 400 nm for 2 days, without other possible adducts detectable (Supporting Information Figs. S1 and S2). Subsequently, with enough **4** and **iii** in hand, the gram-scale synthesis of (±)-**1** was accomplished.

#### 2.4. Inhibition of NO production by compounds **1**–**3**

Because “*yuan hu*” is a wonderful TCM for activating qi and relieving pain, promoting blood circulation and removing blood stasis. As an anti-inflammatory and analgesic ingredient, it is used clinically for the treatment of chest/abdominal pain, injury pain,

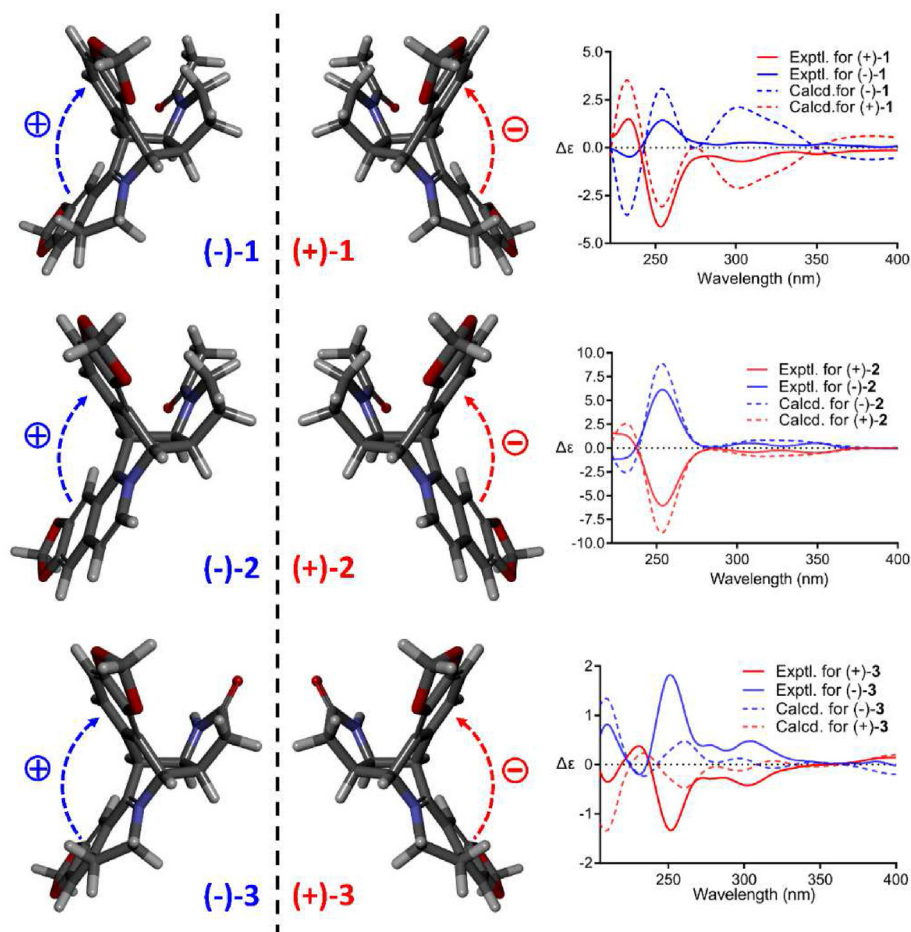


**Figure 4** Split cotton effect and the comparison of experimental and calculated ECD spectra for compounds 1–3.

rheumatism, and so on. Thus, the evaluation of the *in vitro* anti-inflammatory properties of compounds 1–3 were conducted using the assay of LPS-induced NO production in RAW264.7 cells. As a result, compounds 1–3 are more potent than the clinically used agent indomethacin ( $IC_{50} = 15.01 \pm 0.37 \mu\text{mol/L}$ ), with the  $IC_{50}$  values of  $8.72 \pm 0.28$ ,  $3.35 \pm 0.31$ , and  $6.75 \pm 0.91 \mu\text{mol/L}$ , respectively. Furthermore, the ability of down-regulation of the expression of iNOS protein in a dose-dependent manner of ( $\pm$ )-1 was observed in the Western blot analysis (Fig. 5A).

### 2.5. Anti-arthritic effects of compound ( $\pm$ )-1

The anti-arthritic capability of ( $\pm$ )-1 was confirmed *in vivo* using the adjuvant-induced arthritis (AIA) model, a well-established experimental protocol for the study of arthritis and anti-arthritic drugs<sup>39,40</sup>. In this study, ankle circumference (Fig. 5D), hind paw swelling (Fig. 5E) and arthritis index (AI) score (Fig. 5F) were respectively detected to evaluate the therapeutic effects of ( $\pm$ )-1 on rat AIA. As shown in Fig. 5, no significant differences were found in these parameters in all groups before being induced by the complete Freund's adjuvant (CFA). Rats in the CFA immunized groups developed arthritis following the CFA injections. In the treatment group, arthritis progression was significantly suppressed after treatment with ( $\pm$ )-1 at 30 mg/kg for 7 days. Compared with the model group, the hind paw swelling degrees and ankle circumferences were significantly alleviated in

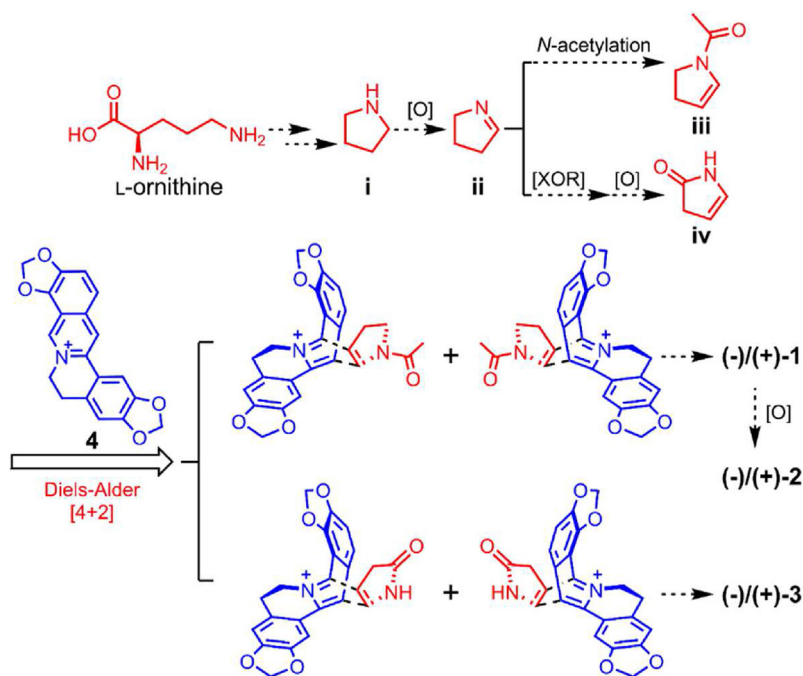
the treatment group. The AI score of the treatment group was reduced to  $11.0 \pm 0.63$  on Day 21. Histopathological examinations of the ankle joint sections of the AIA rats revealed remarkable inflammatory cell infiltration, cartilage destruction, and synovial hyperplasia, in comparison with the synovial joints of the normal rats (Fig. 5G and H). The treatments with ( $\pm$ )-1 demonstrated these pathological events to a significantly lesser degree, a profile similar to that of indomethacin (Indo), a nonsteroidal anti-inflammatory drug. The results indicated that ( $\pm$ )-1 might be a potential agent for relieving arthritis.

### 2.6. Analgesic activity of compound ( $\pm$ )-1

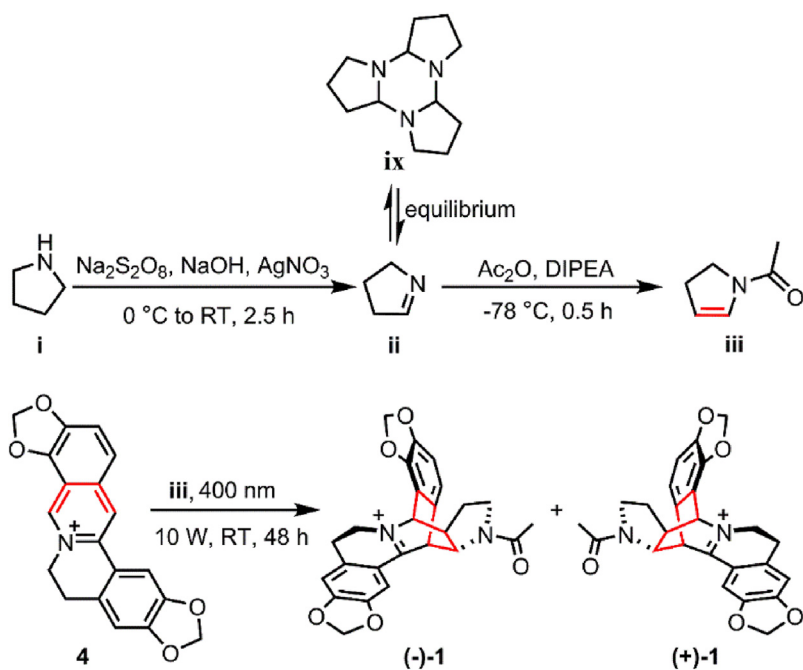
Additionally, the analgesic effect of ( $\pm$ )-1 on acetic acid-induced mice writhing was evaluated in this research. Tetrahydropalmatine (THP), a clinically used analgesic that identified from *C. yanhusuo*, was used as the positive control. As shown in Supporting Information Table S18 and Fig. 5B, ( $\pm$ )-1 demonstrated notable analgesic effect against the acetic acid-induced mice writhing with an inhibition rate of 43.5% at 15.0 mg/kg (i.p.), almost as effective as the positive control. More importantly, dose-dependent inhibitions at 15.0, 45.0, and 67.5 mg/kg (i.p.) were presented by ( $\pm$ )-1.

## 3. Conclusions

Collectively, ( $\pm$ )-yanhusamides A–C (1–3), which possess an unprecedented 3,8-diazatricylco[5.2.2.0<sup>2,6</sup>]undecane-8,10-diene



**Scheme 1** Hypothetical biosynthetic pathway for compounds 1–3.



**Scheme 2** Biomimetic synthesis of compound 1.

core, were isolated from *C. yanhusuo*. The determination of the structural constructions and absolute stereo-chemical configurations of (+)/(-)-1–3 were achieved *via* extensive spectroscopic analysis, GIAO NMR shifts and ECD calculations, and X-ray diffraction analysis. A biomimetic synthesis of ( $\pm$ )-1, involving the use of the key diastereoselective intermolecular DA photocycloaddition at room temperature, has been accomplished. The *in vitro* and *in vivo* anti-inflammatory and analgesic effects of these novel alkaloids further revealed the pharmacodynamic

components of this herbal medicine. Our study not only adds diversity of the bioactive bisbenzylisoquinoline alkaloids (BBIAs), but also provide a convenient chemical method to synthesize benzylisoquinoline-pyrrole dimeric alkaloids. The anti-inflammatory and analgesic effects of ( $\pm$ )-1 support the clinic application of the traditional herbal medicine and provides a new structural architecture of natural products that can be used in follow-up studies relevant to the development of anti-inflammatory and analgesic agents.

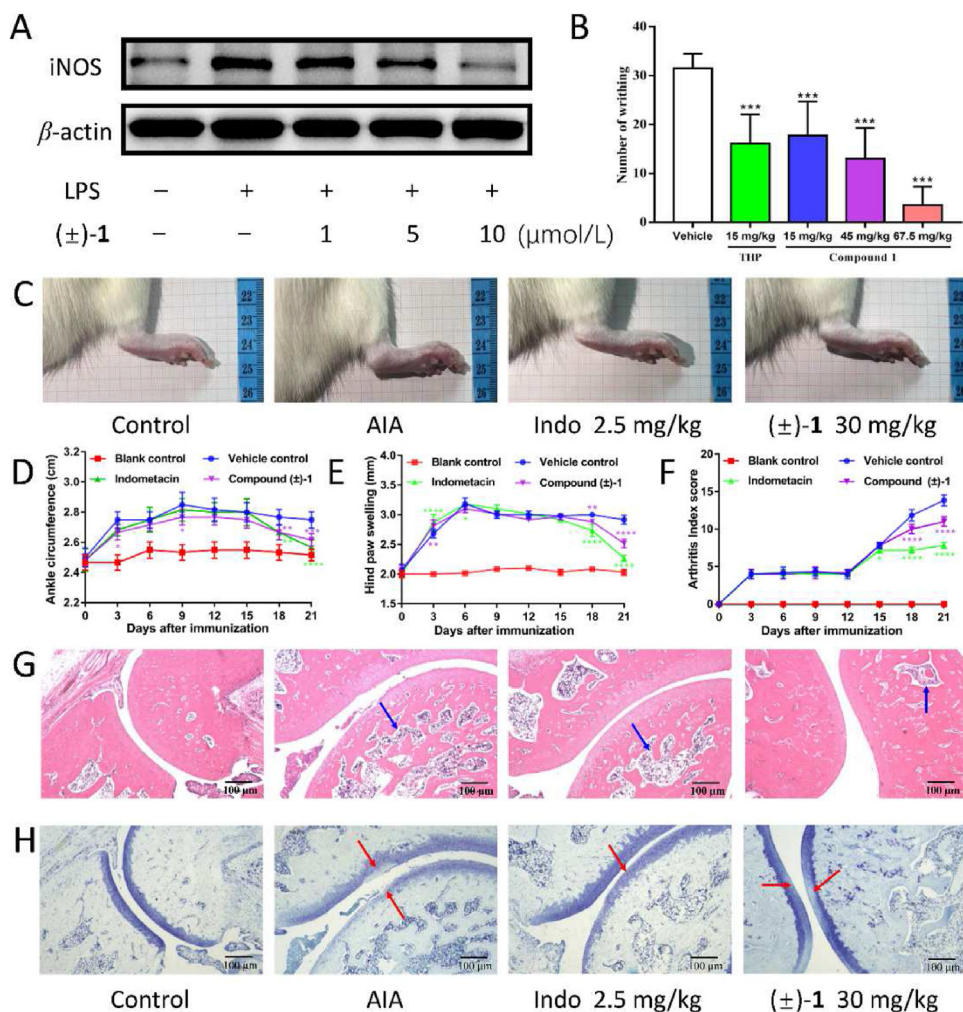


**Figure 5** Analgesic and anti-inflammatory effect of compound (±)-1. (A) Western blot assay of iNOS with the treatment of (±)-1. (B) The analgesic effect of (±)-1 on an animal model of acetic acid-induced writhing assay. (C) Representative macroscopic images of control and inflamed paw images of different groups on Day 21. (D) Ankle circumference. (E) Hind paw swelling. (F) Arthritis index score. (G) Typical images of ankle joint sections with HE staining ( $\times 50$ ), Bar, 100  $\mu\text{m}$ . (H) Typical images of ankle joint sections with toluidine blue staining ( $\times 50$ ), Bar, 100  $\mu\text{m}$ ; The results are shown as mean  $\pm$  SD;  $n = 6$  per group. \* $P < 0.05$ , \*\* $P < 0.01$ , \*\*\* $P < 0.001$ , \*\*\*\* $P < 0.0001$  vs. the vehicle control; The inflammatory cell infiltration is shown as blue arrows, while articular cartilage injury is shown as red arrows.

## 4. Experimental

### 4.1. General experimental procedures

See [Supporting Information](#).

### 4.2. Plant material

See [Ref. 18](#).

### 4.3. Extraction and isolation

For preliminary extraction and fractionation, see [Ref. 17](#). The 50% EtOH fraction (270 g) was subjected to an MCI column chromatography (CC), with MeOH–H<sub>2</sub>O (0%, 40 L; 30%, 100 L; 60%, 100 L; and 95%, 100 L) as eluents to yield four fractions. The 30% MeOH–H<sub>2</sub>O fraction was crystallized in MeOH to give **4** (250 mg). Furthermore, the solution of 30% MeOH–H<sub>2</sub>O fraction (60.2 g) was chromatographed on ODS C<sub>18</sub> column eluting with gradient

MeOH–H<sub>2</sub>O (0–95%), afforded five fractions (FA–FE). Sephadex LH-20 CC was used to preliminary fractionate the FA (19.5 g) eluting with 10% MeOH–H<sub>2</sub>O, led to provide six subfractions (FA1–FA6). Subfraction FA4 (1.7 g) was further separated by an ODS C<sub>18</sub> column eluting with gradient MeOH–H<sub>2</sub>O (0–50%), affording seven fractions (FA41–FA47). Then, the subfraction FA46 (220 mg) was further purified by semipreparative HPLC to give compound **1** [2.0 mg, 254 nm, 250 mm  $\times$  10 mm, RP<sub>18</sub>, 5  $\mu\text{m}$ , CH<sub>3</sub>CN–H<sub>2</sub>O–TFA (25:75:0.1),  $t_R = 11.5$  min] and compound **2** [2.0 mg, 254 nm, 250 mm  $\times$  10 mm, RP<sub>18</sub>, 5  $\mu\text{m}$ , CH<sub>3</sub>CN–H<sub>2</sub>O–TFA (25:75:0.1),  $t_R = 12.7$  min]. Subsequently, compound **1** was further separated by chiral-phase HPLC using an IB-N3 chiral column (254 nm, 250 mm  $\times$  4.6 mm, 3  $\mu\text{m}$ , CH<sub>3</sub>CN–H<sub>2</sub>O–TFA, 40:60:0.05) to afford the anticipated enantiomers (–)-**1** ( $t_R = 6.76$  min) and (+)-**1** ( $t_R = 7.36$  min). Compound **2** was further separated into (–)-**2** ( $t_R = 7.4$  min) and (+)-**2** ( $t_R = 8.1$  min), by the chiral-phase HPLC using the IB-N3 chiral column (254 nm, 250 mm  $\times$  4.6 mm, 3  $\mu\text{m}$ , CH<sub>3</sub>CN–H<sub>2</sub>O–TFA, 40:60:0.05). FA5 (1.9 g) was subsequently separated by an ODS C<sub>18</sub>

column eluting with gradient MeOH–H<sub>2</sub>O (0–50%), to afford nine subfractions (FA51–FA59). Subfraction FA55 (192 mg) was further purified by HPLC to afford compound **3** [4.0 mg, 254 nm, 250 mm × 10 mm, RP<sub>18</sub>, 5 μm, CH<sub>3</sub>CN–H<sub>2</sub>O–TFA (25:75:0.1), *t*<sub>R</sub> = 20.5 min]. Subsequently, compound **3** was separated by HPLC using the IB-N3 chiral column (254 nm, 250 mm × 4.6 mm, 3 μm, CH<sub>3</sub>CN–H<sub>2</sub>O–TFA, 40:60:0.05) to afford the anticipated enantiomers (–)-**3** (*t*<sub>R</sub> = 4.15 min) and (+)-**3** (*t*<sub>R</sub> = 4.35 min).

#### 4.3.1. Yanhusamide A (**1**)

Yellow, amorphous powder; UV (MeOH) λ<sub>max</sub> (log ε) 255 (2.93), 311 (2.51), 377 (2.54) nm; IR (KBr) ν<sub>max</sub> 3406, 2885, 1681, 1628, 1586, 1509, 1468, 1414, 1367, 1344, 1285, 1248, 1204, 1134, 1040, 802, 722 cm<sup>-1</sup>; HRESIMS *m/z* 431.1597 [M]<sup>+</sup> (Calcd. for C<sub>25</sub>H<sub>23</sub>N<sub>2</sub>O<sub>5</sub>, 431.1602); <sup>1</sup>H NMR and <sup>13</sup>C NMR, see Table 1.

(–)-(8*S*,13*S*,2′*S*,3′*R*)-Yanhusamide A [(–)-**1**]: [α]<sub>D</sub><sup>20</sup> –6.7 (*c* 0.05, MeOH); ECD (MeOH) 233 (Δε –0.47), 254 (Δε +1.42), 308 (Δε +0.27), 350 (Δε –0.20).

(+)-(8*R*,13*R*,2′*R*,3′*S*)-Yanhusamide A [(+)-**1**]: [α]<sub>D</sub><sup>20</sup> +10 (*c* 0.07, MeOH); ECD (MeOH) 233 (Δε +1.50), 253 (Δε –4.13), 304 (Δε –0.71), 350 (Δε –0.33).

#### 4.3.2. Yanhusamide B (**2**)

Yellow, amorphous powder; UV (MeOH) λ<sub>max</sub> (log ε) 255 (2.99), 315 (2.45), 349 (2.25) nm; IR (KBr) ν<sub>max</sub> 3457, 3054, 3016, 2907, 2888, 1685, 1631, 1602, 1469, 1447, 1424, 1277, 1205, 1163, 1129, 1047, 1025, 833, 801, 721 cm<sup>-1</sup>; HRESIMS *m/z* 429.1443 [M]<sup>+</sup> (Calcd. for C<sub>25</sub>H<sub>21</sub>N<sub>2</sub>O<sub>5</sub>, 429.1445); <sup>1</sup>H NMR and <sup>13</sup>C NMR, see Table 1.

(–)-(8*S*,13*S*,2′*S*,3′*R*)-Yanhusamide B [(–)-**2**]: [α]<sub>D</sub><sup>20</sup> –15.4 (*c* 0.05, MeOH); ECD (MeOH) 233 (Δε –1.25), 253 (Δε +6.14), 307 (Δε +0.53), 349 (Δε +0.54).

(+)-(8*R*,13*R*,2′*R*,3′*S*)-Yanhusamide B [(+)-**2**]: [α]<sub>D</sub><sup>20</sup> +13.2 (*c* 0.07, MeOH); ECD (MeOH) 233 (Δε +1.20), 253 (Δε –6.04), 310 (Δε –0.42), 349 (Δε –0.49).

#### 4.3.3. Yanhusamide C (**3**)

Yellow, amorphous powder; UV (MeOH) λ<sub>max</sub> (log ε) 203 (3.64), 255 (3.31), 313 (2.90), 378 (3.08) nm; IR (KBr) ν<sub>max</sub> 3413, 3218, 2961, 2923, 2850, 1685, 1583, 1511, 1474, 1459, 1417, 1396, 1342, 1289, 1204, 1136, 1040, 841, 803, 724 cm<sup>-1</sup>; HRESIMS *m/z* 403.1285 [M]<sup>+</sup> (Calcd. for C<sub>23</sub>H<sub>19</sub>N<sub>2</sub>O<sub>5</sub>, 403.1289); <sup>1</sup>H NMR and <sup>13</sup>C NMR, see Table 1.

(–)-(8*S*,13*S*,2′*S*,3′*R*)-Yanhusamide C [(–)-**3**]: [α]<sub>D</sub><sup>20</sup> –14.5 (*c* 0.02, MeOH); ECD (MeOH) 210 (Δε +0.81), 231 (Δε –0.20), 251 (Δε +1.82), 304 (Δε +0.48).

(+)-(8*R*,13*R*,2′*R*,3′*S*)-Yanhusamide B [(+)-**3**]: [α]<sub>D</sub><sup>20</sup> +15.0 (*c* 0.01, MeOH); ECD (MeOH) 210 (Δε –0.35), 231 (Δε +0.38), 251 (Δε –1.34), 302 (Δε –0.43).

#### 4.3.4. In silico prediction of <sup>13</sup>C NMR chemical shifts and ECD spectrum of **1–3**

See Supporting Information.

#### 4.3.5. Biomimetic experimental procedures for compound **1**

See Supporting Information.

#### 4.4. In vitro anti-inflammatory assay

The preliminary *in vitro* anti-inflammatory activities of compounds **1–3** were tested by applying the assay of NO production induced by LPS in the RAW264.7 macrophages as described in the Supporting Information.

#### 4.5. In vivo biological protocols

##### 4.5.1. Effects of (±)-**1** on rats with AIA

The AIA model of rats was induced according to the protocol described previously<sup>40,41</sup>. Briefly, 0.1 mL commercial CFA (Beyotime, China) was injected intradermally into the right hind paw of Sprague–Dawley rats (Day 0). Rats in blank control received a single intradermal injection of 0.1 mL of blank oil–water emulsion. Immunized rats were given by gastric gavage of (±)-**1** (30.0 mg/kg per day) from Day 15 after the induction and daily for the next 7 days (test group). Rats in the positive and blank control groups received 2.5 mg/kg per day of indomethacin and isopyknic normal saline, respectively, during the same period of the test group. Prior to the immunization and every three days after the immunization up to 21 day (Day 21), clinical evaluation was performed through measurement of edema, standardized scoring of arthritis, and pathological section staining as described previously<sup>41</sup>.

##### 4.5.2. Acetic acid-induced writhing assay

The acetic acid-induced writhing tests were carried out according to the protocol described previously<sup>42,43</sup>. Generally, Fifty IRC female mice were randomly divided into five groups. Mice in the vehicle and positive groups were pretreated intraperitoneally with normal saline and tetrahydropalmatine (15.0 mg/kg), respectively. Mice in the three test groups were pretreated intraperitoneally with (±)-**1** (15.0, 45.0 and 67.5 mg/kg, respectively). 30 min after the administration, each mouse received a single dose of 1.0% *v/v* acetic acid solution (0.1 mL/kg) by intraperitoneal injection. The writhing numbers of the mice in the following 15 min were recorded. Subsequently, the analgesic effects of tetrahydropalmatine and different dose of (±)-**1** were respectively expressed by the reducing of the writhing numbers compared to normal saline. Percent inhibitions were calculated using Eq. (1):

$$\text{Percent inhibition (\%)} = [(W_m - W_t)/W_m] \times 100 \quad (1)$$

where *W*<sub>m</sub> represents the writhing number of the vehicle group, and *W*<sub>t</sub> represents the writhing number of test groups or positive group.

All animal experiments were approved by the Animal Research Ethics Board of Dongzhimen Hospital, Beijing, China.

#### Acknowledgments

This study was supported by the National Natural Science Foundation of China (No. 82073978), Beijing Natural Science Foundation (No. JQ18026, China), and the Fundamental Research Funds for the Central Universities (2022-JYB-JBZR-015, China).

### Author contributions

Prof. Dr. Sheng Lin initiated and coordinated the project. Dr. Lingyan Wang carried out the study and collected important background information. Dr. Lingyan Wang and Dr. Guiyang Xia performed the experiments. Dr. Huan Xia and Dr. Xiaohong Wei provided assistance for compound characterization and data analysis. Dr. Yanan Wang contributed to carry out the 1D- and 2D-NMR spectra data. Prof. Dr. Sheng Lin performed manuscript revision. All authors contributed to manuscript revision, read, and approved the submitted version.

### Conflicts of interest

The authors declare no conflicts of interest.

### Appendix A. Supporting information

Supporting data to this article can be found online at <https://doi.org/10.1016/j.apsb.2022.10.025>.

### References

- Peixoto PA, El Assal M, Chataigner I, Castet F, Cornu A, Coffinier R, et al. Bispericyclic Diels–Alder dimerization of *ortho*-quinols in natural product (bio)synthesis: bioinspired chemical 6-step synthesis of (+)-maytenone. *Angew Chem Int Ed Engl* 2021;**60**:14967–74.
- Gomes NGM, Pereira RB, Andrade PB, Valentao P. Double the chemistry, double the fun: structural diversity and biological activity of marine-derived diketopiperazine dimers. *Mar Drugs* 2019;**17**:551.
- Liu J, Liu A, Hu Y. Enzymatic dimerization in the biosynthetic pathway of microbial natural products. *Nat Prod Rep* 2021;**38**:1469–505.
- Wang W, Xiong L, Wu Y, Zhou Y, Li Y, Zheng M, et al. New lathyrane diterpenoid hybrids have anti-inflammatory activity through the NF- $\kappa$ B signaling pathway and autophagy. *Acta Mater Med* 2022;**1**:224–43.
- Wang G, Li L, Wang X, Li X, Zhang Y, Yu J, et al. Hypericin enhances beta-lactam antibiotics activity by inhibiting sarA expression in methicillin-resistant *Staphylococcus aureus*. *Acta Pharm Sin B* 2019;**9**:1174–82.
- Zhang J, Gao L, Hu J, Wang C, Hagedoorn PL, Li N, et al. Hypericin: source, determination, separation, and properties. *Sep Purif Rev* 2020;**51**:1–10.
- O'Connor SE, Maresh JJ. Chemistry and biology of monoterpene indole alkaloid biosynthesis. *Nat Prod Rep* 2006;**23**:532–47.
- Shen S, Tong Y, Luo Y, Huang L, Gao W. Biosynthesis, total synthesis, and pharmacological activities of aryltetralin-type lignan podophyllotoxin and its derivatives. *Nat Prod Rep* 2022;**39**:1856–75.
- Liu Y, Wang L, Zhao L, Zhang Y. Structure, properties of gossypol and its derivatives—from physiological activities to drug discovery and drug design. *Nat Prod Rep* 2022;**39**:1282–304.
- Hostalkova A, Marikova J, Opletal L, Korabecny J, Hulcova D, Kunes J, et al. Isoquinoline alkaloids from *Berberis vulgaris* as potential lead compounds for the treatment of Alzheimer's Disease. *J Nat Prod* 2019;**82**:239–48.
- Bracher F, Eisenreich WJ, Muhlbacher J, Dreyer M, Bringmann G. Saludimerines A and B, novel-type dimeric alkaloids with stereogenic centers and configurationally semistable biaryl axes. *J Org Chem* 2004;**69**:8602–8.
- Wei HL, Han Y, Zhou H, Hou T, Yao YM, Wen CM, et al. Isoquinoline alkaloid dimers with dopamine D1 receptor activities from *Menispermum dauricum* DC. *Phytochemistry* 2022;**194**:113015.
- Sai CM, Li DH, Xue CM, Wang KB, Hu P, Pei YH, et al. Two pairs of enantiomeric alkaloid dimers from *Macleaya cordata*. *Org Lett* 2015;**17**:4102–5.
- Li DH, Li JY, Xue CM, Han T, Sai CM, Wang KB, et al. Anti-proliferative dimeric aporphinoid alkaloids from the roots of *Thalictrum cultratum*. *J Nat Prod* 2017;**80**:2893–904.
- Bhagya N, Chandrashekar KR. Tetrandrine—a molecule of wide bioactivity. *Phytochemistry* 2016;**125**:5–13.
- Yang Y, Yang P, Huang C, Wu Y, Zhou Z, Wang X, et al. Inhibitory effect on SARS-CoV-2 infection of neferine by blocking Ca<sup>2+</sup>-dependent membrane fusion. *J Med Virol* 2021;**93**:5825–32.
- Wang LY, Qiu BL, Xia H, Xia GY, Xiao BB, Zhang JF, et al. Yanhusanines A–F, isoquinoline-derived alkaloid enantiomers from *Corydalis yanhusuo* and their biological activity. *J Nat Prod* 2020;**83**:489–96.
- Xia GY, Fang DJ, Wang LY, Xia H, Wang YN, Shang HC, et al. 13,13a-*seco*-Protoberberines from the tubers of *Corydalis yanhusuo* and their anti-inflammatory activity. *Phytochemistry* 2022;**194**:113023.
- Xia GY, Xiao BB, Wang LY, Fang DJ, Xia H, Lin S. A new dimeric benzylisoquinoline alkaloid from *Corydalis yanhusuo*. *Acta Pharm Sin* 2021;**56**:553–6.
- Xiao BB, Xia GY, Wang LY, Qiu BL, Xia H, Zhong WC, et al. (±)-Bicoryanahunine A, dimeric benzylisoquinoline alkaloid atropenantiomers from *Corydalis yanhusuo*. *Tetrahedron Lett* 2020;**61**:151890.
- Raja SN, Carr DB, Cohen M, Finnerup NB, Flor H, Gibson S, et al. The revised international association for the study of pain definition of pain: concepts, challenges, and compromises. *Pain* 2020;**161**:1976–82.
- Finckh A, Gilbert B, Hodkinson B, Bae SC, Thomas R, Deane KD, et al. Global epidemiology of rheumatoid arthritis. *Nat Rev Rheumatol* 2022;**18**:591–602.
- Tamura T, Ohmori K. Diacerein suppresses the increase in plasma nitric oxide in rat adjuvant-induced arthritis. *Eur J Pharmacol* 2001;**419**:269–74.
- Soos B, Szentpetery A, Raterman HG, Lems WF, Bhattoa HP, Szekanez Z. Effects of targeted therapies on bone in rheumatic and musculoskeletal diseases. *Nat Rev Rheumatol* 2022;**18**:249–57.
- Fang DJ, Xia GY, Wang LY, Xia H, Sun YB, Lin S. A new dimeric dehydrocorydaline alkaloid from vinegar-prepared *Corydalis yanhusuo*. *Acta Pharm Sin* 2021;**56**:1096–9.
- Finefield JM, Sherman DH, Kreitman M, Williams RM. Enantiomeric natural products: occurrence and biogenesis. *Angew Chem Int Ed Engl* 2012;**51**:4802–36.
- Xia GY, Wang LY, Xia H, Wu YZ, Wang YN, Hu HY, et al. Circularly polarized luminescence of talarolactones (+)(–)-A and (+)(–)-C: the application of CPL-calculation in stereochemical assignment. *Chin Chem Lett* 2022;**33**:4253–6.
- Cheng MJ, Yang XY, Cao JQ, Liu C, Zhong LP, Wang Y, et al. Isolation, structure elucidation, and total synthesis of Myrtospirone A from *Myrtus communis*. *Org Lett* 2019;**21**:1583–7.
- Zou CX, Wang XB, Lv TM, Hou ZL, Lin B, Huang XX, et al. Flavan derivative enantiomers and drimane sesquiterpene lactones from the *Inonotus obliquus* with neuroprotective effects. *Bioorg Chem* 2020;**96**:103588.
- Zhang S, Yang Q, Guo L, Zhang Y, Feng L, Zhou L, et al. Isolation, structure elucidation and racemization of (+)- and (–)-pratsilins A–C: unprecedented spiro indolinone-naphthofuran alkaloids from a marine *Streptomyces* sp. *Chem Commun* 2017;**53**:10066–9.
- Karadogan B, Parsons PJ. Synthesis of racemic brevioxime and related analogues. *Tetrahedron* 2001;**57**:8699–703.
- Kraus GA, Neuenschwander K. Facile synthesis of *N*-acyl-2-pyrrolines. *J Org Chem* 2002;**46**:4791–2.

33. Zhao T, Kurpiewska K, Kalinowska-Tluscik J, Herdtweck E, Domling A. Alpha-amino acid-isosteric alpha-amino tetrazoles. *Chem Eur J* 2016;**22**:3009–18.
34. Qin DP, Pan DB, Xiao W, Li HB, Yang B, Yao XJ, et al. Dimeric cadinane sesquiterpenoid derivatives from *Artemisia annua*. *Org Lett* 2018;**20**:453–6.
35. Cao W, Dou Y, Kouklovsky C, Vincent G. Total synthesis of Ophiorrhine A, G and Ophiorrhside E featuring a bioinspired intramolecular Diels–Alder cycloaddition. *Angew Chem Int Ed Engl* 2022;**61**:e202209135.
36. Li C, Li CJ, Ma J, Chen FY, Li L, Wang XL, et al. Magterpenoids A–C, three polycyclic meroterpenoids with PTP1B inhibitory activity from the bark of *Magnolia officinalis* var. *biloba*. *Org Lett* 2018;**20**:3682–6.
37. Romero NA, Nicewicz DA. Organic photoredox catalysis. *Chem Rev* 2016;**116**:10075–166.
38. Kumar GS, Lin Q. Light-triggered click chemistry. *Chem Rev* 2021;**121**:6991–7031.
39. Wang Q, Qin X, Fang J, Sun X. Nanomedicines for the treatment of rheumatoid arthritis: state of art and potential therapeutic strategies. *Acta Pharm Sin B* 2021;**11**:1158–74.
40. Grottsch B, Bozec A, Schett G. Methods in molecular biology. In: Idris A, editor. *Bone research protocols*. New York: Humana Press; 2019. p. 269–80.
41. Yang J, Cai HD, Zeng YL, Chen ZH, Fang MH, Su YP, et al. Effects of koumine on adjuvant- and collagen-induced arthritis in rats. *J Nat Prod* 2016;**79**:2635–43.
42. Guo Q, Xia H, Wu Y, Shao S, Xu C, Zhang T, et al. Structure, property, biogenesis, and activity of diterpenoid alkaloids containing a sulfonic acid group from *Aconitum carmichaelii*. *Acta Pharm Sin B* 2020;**10**:1954–65.
43. Wu Y, Shao S, Guo Q, Xu C, Xia H, Zhang T, et al. Aconicatisulfonines A and B, analgesic zwitterionic C<sub>20</sub>-diterpenoid alkaloids with a rearranged atisane skeleton from *Aconitum carmichaelii*. *Org Lett* 2019;**21**:6850–4.